SUPPRESSION EFFECTS OF TYPICAL INERT GASES ON THE EXPLOSION CHARACTERISTICS OF GASOLINE MIST IN CLOSED VESSEL

Run Li[a], Yangfan Cheng[a,b,*], Haojian Liang[b], Zihan Chen[b], Jianwei Xu[b], Wenxin Wang[b]

[a] *School of Safety Science and Engineering, Anhui University of Science and Technology, Huainan 232001, PR China*

[b] *School of Chemical and Blasting Engineering, Anhui University of Science and Technology, Huainan, 232001, Anhui, China*

[*]Corresponding authors; Email: cyf518@mail.ustc.edu.cn

Gasoline presents considerable safety hazards during the storage and transportation processes. In the study, the effects of three typical inert gases of carbon dioxide (CO_2), nitrogen (N_2), and argon (Ar) on the cloud explosion of gasoline were studied using a 20 L spherical explosion vessel. The experimental results showed that the ultimate volume fractions (n_U) of the inert gases required to completely suppress gasoline cloud explosion were 86 vol. %, 88 vol. %, and 92 vol. %, respectively. As the volume fraction (n) of inert gases increased, the maximum explosion pressure (ΔP_{max}), the maximum explosion pressure rise rate ($(dP/dt)_{max}$), the maximum average temperature (T_{am}), and the explosion risk index (K_G) of the gasoline cloud explosion all exhibited a downward trend, while the combustion duration (t_d) increased. CO_2 primarily inhibited the initial stage of the gasoline cloud explosion reaction, reducing the oxidation rate by interfering with elementary reactions through both physical (heat absorption) and chemical (reaction inhibition) ways. While N_2 and Ar mainly weakened the second stage of explosion, primarily through heat absorption and dilution effects. The research conclusions could offer theoretical guidance for the safe storage and transportation of gasoline by making explosion protection measures.

Keywords: *Gasoline; cloud explosion; inert gases; explosion suppression; flame temperature*

1. Introduction

Gasoline is a complex mixture consisting of light components, including aromatic hydrocarbons, saturated hydrocarbons, and cycloalkanes. It is extensively used in transportation and energy production. Currently, commercially available gasoline is derived from petroleum through processes such as fractionation and catalytic cracking. At standard temperature and pressure, gasoline exists in a liquid state. Its energy content surpasses that of certain gaseous fuels, and it is more convenient to be processed and transported compared to solid fuels. Gasoline is predominantly employed in internal combustion engine systems due to its cost-effectiveness, broad applicability, and consistent power output, while the toxic and harmful byproducts generated during combustion are relatively minimal. Nevertheless, gasoline mist leakage and the atomization of liquid fuel could result in the formation of a combustible mixture when mixed with air. This mixture poses significant safety risks, as it could lead to fire, explosion, and other hazardous incidents once contact with ignition sources.

Explosion characteristic parameters, including explosion pressure, explosion pressure rise rate, combustion duration, and explosion index, are essential for assessing the risk associated with fuel mist and

cloud explosions. Zahlanieh et al. [1] investigated the impact of mist fraction on the explosion characteristic parameters of mixed fuels, including isooctane, Jet A1 aviation fuel, and diesel fuel using a 20 L spherical explosive vessel, and they proposed a testing methodology for evaluating the flammability and explosion risk of mixed clouds. Cai et al. [2] examined the effects of initial turbulence and equivalence ratio on the explosion characteristic parameters of liquefied petroleum gas and dimethyl ether clean mixed fuel through experimental studies. Their findings revealed that both the maximum explosion pressure and the maximum pressure rise rate exhibited a nearly linear relationship with initial turbulence. In a simulation of the gas-liquid two-phase explosion of n-heptane in the premixed region, Song et al. [3] identified a significant secondary explosion phenomenon occurring outside the premixed region. Yang et al. [4] explored the coupling effects of low temperature and low pressure on high volatile liquid fuels using a 20 L spherical explosion vessel. Their results demonstrated that as ambient temperature or pressure decreased, the explosion pressure and the explosion pressure rise rate initially increased before subsequently decreasing. Additionally, they established predictive equations for the explosion pressure and combustion duration.

In view of the danger of liquid fuel in explosion, numerous scholars have conducted in-depth research on related safety concerns [5,6]. The traditional explosion suppression method is to suppress the explosion of dangerous procedures or items by adding solid explosion suppressors [7,8], liquid explosion suppressors [9] and inert gases [10]. However, for liquid fuels, the addition of solid explosion suppressors (carbonates, phosphates, halides, etc.) [11,12] and liquid explosion suppressors (hydrocarbon liquids, fluorides, oxalate liquids, etc.) [13,14] , will affect the physical and chemical properties of liquid fuels themselves, and even increase their explosion risk [15]. While the addition of inert gases will not change the composition of the liquid, resulting in a better explosion suppression effect. Abdelkhalik et al. [16] conducted a comparative analysis of the inerting effects of four inert gases on propane, acetone, isopropanol and methyl acetate fuels by experimental and numerical simulation methods, and found that the order of explosion suppression effect was CO_2 > He > N_2 > Ar. Mitu [17] studied the effects of N_2, exhaust gas, H_2O and CO_2 on the explosion characteristics of ethanol solution under closed condition, and found that the order of explosion suppression effect was CO_2 > H_2O (g) > exhaust gas > N_2. Luo et al. [18] investigated the influence of inert gases on the mixed explosion of liquefied petroleum gas and air, concluding that when the proportion of liquefied petroleum gas was relatively low, the inhibition effect of CO_2 was better than that of N_2, while when the proportion of liquefied petroleum gas was relatively high, the conclusion was the opposite.

Current studies on gasoline fuel predominantly emphasizes the design of gasoline storage tanks, the analysis of gasoline composition, and the numerical simulation of gasoline mist explosions. Significant investigations have been conducted regarding the oxidation reactions, evaporation characteristics, and burning properties of alternative fuels during the combustion processes [19-22]. However, there are few studies addressing the inhibition mechanisms of inert gases on gasoline fuel explosions. This study investigated the effects of three typical inert gases on the deflagration characteristics of gasoline cloud in a confined condition, and reconstructed the temperature field of the gasoline flames with the addition of different inert gases. Furthermore, the inhibition mechanisms of three typical inert gases for the gasoline flames were discussed.

2. Experimental materials and apparatus

2.1 Experimental materials

The gasoline used in the experiment was produced by the China National Petroleum Corporation. Four gases of O_2, N_2, Ar, and CO_2 (purity ≥ 99.9 %) were supplied by Hefei Henglong Electric Co., Ltd.

2.2 Experimental apparatus and procedures

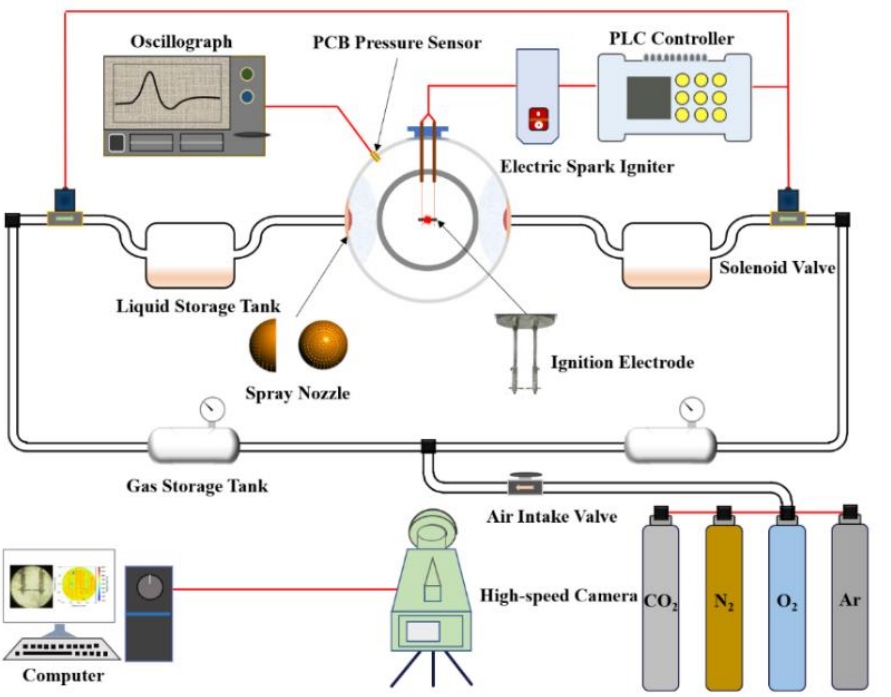

Figure 1. Schematic of the 20-L liquid fuel explosion test system

The apparatus used in the experiment was a 20 L spherical explosion vessel, manufactured by China Jilin Hongyuan Scientific Instrument Co., Ltd. As illustrated in Fig. 1, the measuring system was primarily composed of a 20 L spherical explosion tank, a fuel spraying system, an ignition system, a data acquisition system, and a synchronous control system. The front section of the tank features an optical observation window with a diameter of 14 cm, facilitating the capture of flame morphology by a high-speed camera (Memrecam HX 3, NAC, Japan). The fuel spraying system consisted of two dispersion nozzles, two 70 ml fuel storage tanks, two electromagnetic control valves, two 1.5 L gas storage tanks, and four high-pressure gas cylinders. The ignition system contained two pure tungsten electrodes separated by a gap of 1.5 mm, along with an electric spark generator. The electric spark generator employed in this experiment operates through a continuous pulse circuit. The data acquisition system included a PCB pressure sensor (PCB 113B24, USA) and an oscilloscope (Teledyne Lecroy, HDO4034, USA). The synchronous control system incorporated a programmable logic controller (PLC, Foshan Minkong Technology Co., Ltd., China) to regulate the fuel spraying duration and ignition delay time. Before ignition, air with a pressure of 0.8 MPa was pumped into a gas storage tank, and the fuel spraying duration was set to 100 ms to ensure complete atomization of the liquid into the spherical tank. The experiments were conducted at the room temperature (298 K) and atmospheric pressure (0.1 MPa). The electronic vacuum gauge used for gas distribution had an accuracy of ±0.04 kPa. Each experimental condition was replicated a minimum of three times to minimize experimental error[23].

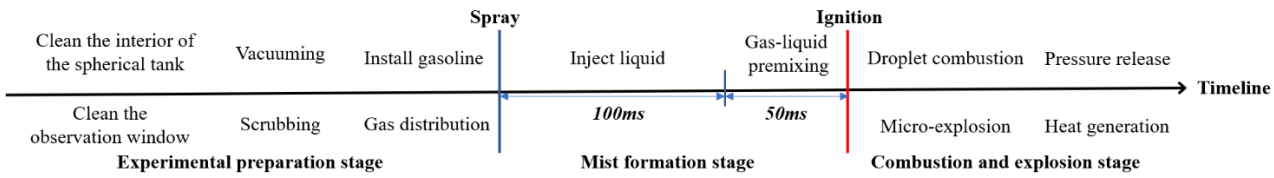

Figure 2. Timing diagram of experimental operation

The 20 L spherical liquid explosion test experiment primarily comprised three stages: the experimental preparation stage, the mist formation stage, and the explosion stage. As illustrated in Fig. 2, before the experiment, the vessel must be thoroughly cleaned, ventilated, and cooled. Subsequently, gasoline was

introduced into the liquid storage tank, and the ball cap was sealed to create a vacuum of -0.1 MPa. After that, an inert gas-oxygen mixture was pumped with a controlled proportion into both the spherical tank and the jet tank. Once these operations were completed, the internal gases were allowed to be premixed for a duration of five minutes. Upon activation of the switch, the jet tank operated continuously for 100 ms, facilitating the transfer of gasoline from the liquid storage tank into the spherical tank. This process was followed by an automatic ignition after a 50 ms cloud formation period, resulting in the combustion and explosion of the gasoline cloud in the confined space.

3. Results and discussion

3.1 Ultimate Inert Volume Fraction (n_U) of Gasoline Cloud Explosion

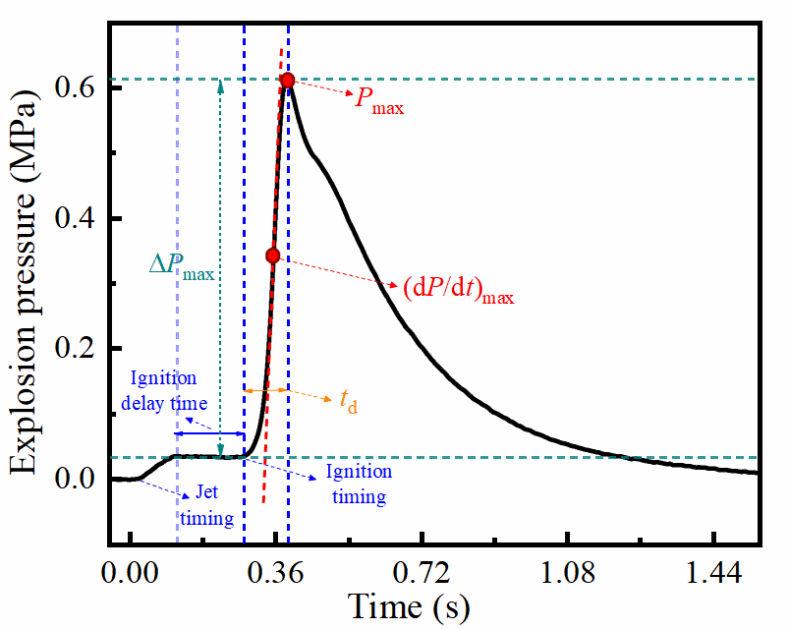

Figure 3. Definition diagram of characteristic parameters for explosion pressure curves

Gasoline is characterized as a highly volatile liquid fuel, exhibiting reduced volatility within the temperature range of 30 to 80 °C. However, when the ambient temperature surpasses 80 °C, gasoline demonstrates significant volatility. In the experiment, the mass concentration of gasoline was maintained at a fixed value of 200 g/m³. Following a series of spray non-ignition tests, it was observed that due to losses associated with the pipe wall [24], the actual mass concentration of gasoline injected was measured at 160 g/m³. Fig. 3 was a typical gasoline cloud explosion pressure time history curve. Due to the injection of high-pressure gas during the fuel spraying process, pressure fluctuation appeared in the initial stage of pressure rise, and the moment when the fluctuation started was defined as the jet timing. Subsequently, there was a platform area in the pressure curve before the explosion pressure began to rise. The time period corresponding to the platform was consistent with the ignition delay time of this experiment. Therefore, the time when the pressure began to rise was determined as the ignition timing. The apex of the curve was defined as the apparent maximum pressure (P_{max}) of the gasoline explosion, and the difference between the maximum explosion pressure and the explosion pressure at the ignition time was regarded as the actual maximum pressure (ΔP_{max}). The interval between the ignition timing and the corresponding moment of the apparent maximum pressure (P_{max}) was termed the combustion duration (t_d). The volume fraction of inert gas that completely inhibits gasoline cloud explosion is the final volume fraction of inert gas (n_U). Furthermore, the maximum slope of the

curve during the gasoline explosion pressure rise was defined as the maximum explosion pressure rise rate ($(dP/dt)_{max}$).

The flammability limit value is a critical parameter for assessing the susceptibility of combustible materials to explosion. The principle of inert gas suppression for combustible materials is to control the proportion of inert gas above the limit inerting volume fraction. Based on the flammability limit testing method and the criteria for gas-liquid two-phase material explosions, the standards for determining an explosion can be outlined as follows [25,26]: (1) pressure standard: a change in internal pressure exceeding 5 %, accompanied by a continuous upward trend; (2) flame standard: the presence of a distinct flame or flame core at the ignition electrode, as captured by a high-speed camera. The n_U of inert gas in relation to gasoline cloud explosions was evaluated using the up-and-down method. A minimum of five parallel tests were conducted for each sample to ascertain the success of ignition, and symbolized successful and unsuccessful ignition as *S* and *F*, respectively. For illustrative purposes, the test results obtained in a CO_2 atmosphere were presented in Table 1 and Fig. 4, which showed the corresponding pressure data and flame propagation characteristics.

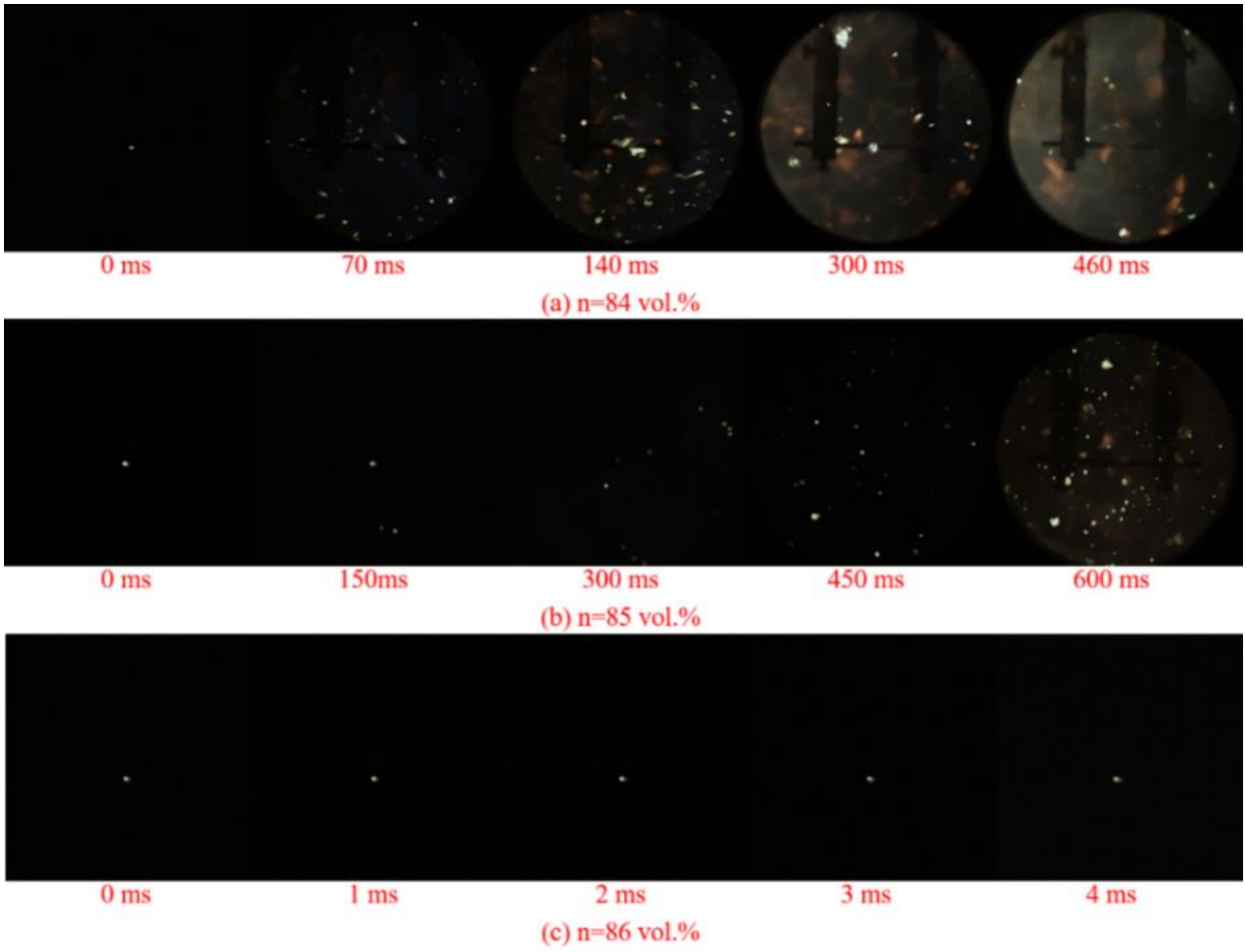

Figure 4. Flame propagation processes of gasoline cloud in CO_2 atmosphere

The results indicated that at a volume fraction of *n*=84 vol. % of CO_2, the gasoline cloud could be reliably ignited, allowing for the flame propagation. In contrast, at *n*=85 vol. %, ignition was successfully achieved in only one experiment, with a maximum explosion pressure (ΔP_{max}) of 0.42 MPa, and only weak flame propagation was observed. At *n*=86 vol. %, neither pressure fluctuation nor flame propagation occurred. Continuous testing was conducted on three gases (CO_2, N_2, Ar) mixed with O_2 to ascertain the maximum volume fraction of inert gas (n_U) capable of completely suppressing the gasoline cloud explosion. The volume fraction of inert gas (*n*) was incrementally increased by 1 vol. % interval from initial value of 79 vol. % (approximately the proportion of N_2 in ambient air) until the complete suppression of the gasoline cloud

explosion was achieved. The results of these tests were presented in Table 2. The data indicated that n_U for the suppression of gasoline cloud explosion using CO_2, N_2, and Ar were 86 vol. %, 88 vol. %, and 92 vol. %, respectively.

Table 1 The n_U test results under CO_2 atmosphere.

n (vol. %)	ΔP_{max} (MPa)	S (Success)/F (Failure)
83	0.63	5 (S)
84	0.57	5 (S)
85	0.42	1 (S) and 4 (F)
86	-	5 (F)
87	-	5 (F)

Table 2 Continuous testing of limit inert gases fraction.

n (vol. %)	CO_2	N_2	Ar
79	5 (S)	5 (S)	5 (S)
80	5 (S)	5 (S)	5 (S)
81	5 (S)	5 (S)	5 (S)
82	5 (S)	5 (S)	5 (S)
83	5 (S)	5 (S)	5 (S)
84	5 (S)	5 (S)	5 (S)
85	1 (S) and 4 (F)	5 (S)	5 (S)
86	5 (F)	5 (S)	5 (S)
87	5 (F)	2 (S) and 3 (F)	5 (S)
88	–	5 (F)	5 (S)
89	–	5 (F)	5 (S)
90	–	–	5 (S)
91	–	–	2 (S) and 3 (F)
92	–	–	5 (F)
93	–	–	5 (F)

3.2 Influences of inert gases on explosion characteristic parameters

Fig. 5 illustrated the variations in the deflagration characteristic parameters of gasoline as the value of volume fraction of inert gas (n) increased under the influence of CO_2, N_2, and Ar. The data presented in Fig. 5 indicated that, in the three types of atmospheres, both ΔP_{max} and $(dP/dt)_{max}$ of gasoline explosions exhibited a downward trend with the increasing volume fraction of inert gas (n), while T_d showed an upward trend. In CO_2 atmosphere, as volume fraction of inert gas (n) increased from 79 vol. % to 84 vol. %, ΔP_{max} and $(dP/dt)_{max}$ decreased by 35 % and 86 %, respectively, while T_d increased by 322 %. In N_2 atmosphere, as n rose from 79 vol. % to 86 vol. %, ΔP_{max} and $(dP/dt)_{max}$ decreased by 33 % and 77 %, respectively, while T_d increased by 418 %. In Ar atmosphere, as volume fraction of inert gas (n) increased from 79 vol. % to 90 vol. %, ΔP_{max} and $(dP/dt)_{max}$ decreased by 36 % and 87 %, respectively, while t_d increased by 343 %. These results demonstrated that all of the three atmospheres exerted an inhibitory effect on the pressure change associated with gasoline cloud explosions, with Ar exhibiting a relatively broader range of inhibition and necessitating a higher proportion of inert gas.

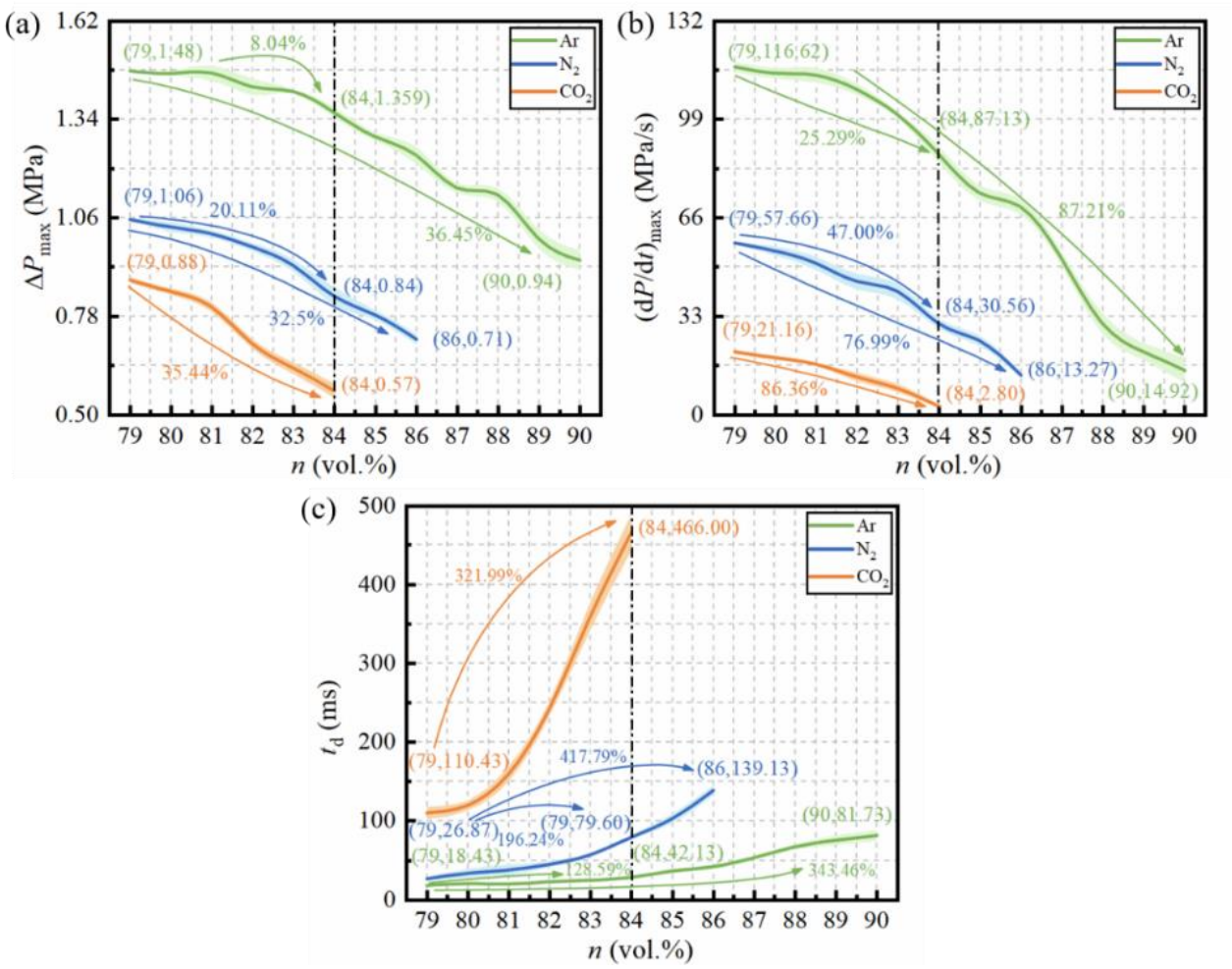

Figure 5. Comparison of gasoline cloud under three different inert gases with varying volume ratios: (a) ΔP_{max}; (b) $(dP/dt)_{max}$; (c) t_d.

In the same range of volume fraction of inert gas (n) from 79 to 84 vol. %, ΔP_{max} and $(dP/dt)_{max}$ decreased by 35.44 % and 86.36 %, respectively, while T_d increased by 321.99 % in CO_2 atmosphere. In N_2 atmosphere, ΔP_{max} and $(dP/dt)_{max}$ decreased by 20.11 % and 47.00 %, respectively, while T_d increased by 196.24 %. In Ar atmosphere, ΔP_{max} and $(dP/dt)_{max}$ decreased by 8.04 % and 25.29 %, respectively, while T_d increased by 128.59 %. These results indicated that the inhibitory effects of the three inert gases on gasoline explosions followed the order of $CO_2 > N_2 > Ar$.

This phenomenon was associated with the specific heat capacity of inert gases. For various inert gases, a larger specific heat capacity correlates with a greater absorption of heat generated during the deflagration processes. Consequently, at the same concentration, CO_2 exhibited a more pronounced inhibitory effect on gasoline cloud explosion, leading to smaller values of ΔP_{max} and $(dP/dt)_{max}$[27].

$$K_G = \left(\frac{dP}{dt}\right)_{max} \cdot V^{\frac{1}{3}} \quad (1)$$

Table 3 Classification for K_G.

No.	K_G (MPa·m/s)	Classification	Risk
1	0	St0	Non-explosible
2	0-20	St1	Weak
3	20-30	St2	Strong
4	>30	St3	Very Strong

The variation of K_G value for gasoline cloud explosion under different volume fractions of inert gas was presented and Table 3 provided the classification of K_G[28]. As *n* of the three inert gases increased, the risk of gasoline cloud explosions gradually decreased. In CO_2 atmosphere, as *n* increased from 79 vol. % to 84 vol. %, the K_G value decreased from 5.74 MPa·m/s to 0.76 MPa·m/s, representing a reduction of 87 %. Within this concentration range, the gasoline cloud explosion was classified as St1. When *n* exceeded 86 vol. %, the explosion was completely suppressed, resulting in a K_G value of 0. Similarly, in N_2 atmosphere, the risk of gasoline cloud explosions within the tested range was also categorized as St1. As *n* increased from 79 vol. % to 86 vol. %, the K_G value decreased by 77 %. When *n* was larger than 88 vol. %, K_G value was 0. In the case of Ar atmosphere, the risk of gasoline cloud explosion within the tested range experienced three stages. When *n* is between 79 and 81 vol. %, the explosion risk was classified as St3. The *n* values corresponding to the St2 and St1 stages were in the ranges of 81-85 vol. % and 85-90 vol. %, respectively. Compared to the addition of inert gases at the same volume fraction from 79 vol. % to 84 vol. %, the K_G values in the three atmospheres decreased by 86 %, 47 %, and 25 %, respectively, which indicated that the inhibitory effect of CO_2 on the explosion index was more pronounced, while the inhibitory effect of Ar was the weakest.

According to equation (1), when the volume of the explosion vessel remained constant, the explosion index was closely related to the maximum pressure rise rate during the explosion. Factors such as the concentration of combustibles, the concentration of oxidants, ambient temperature, ambient pressure, and the contact area between combustibles and oxidants would significantly influence the explosion pressure and the explosion pressure rise rate [29-31]. This study had consistently been explored under room temperature and pressure conditions. Under specific circumstances, when the gasoline cloud concentration, O_2 content and *n* value were kept constant, the primary factor affecting K_G was the contact area between the gasoline cloud and O_2. The results indicated that among the three inert gases, CO_2 significantly reduced the contact area between combustibles and oxygen. Furthermore, the gasoline mist explosion reaction was a chain reaction initiated by direct oxidation.

When gasoline mist exploded, the light components reacted with O_2 to produce H_2O and intermediate products and released large amounts of heat. The heat promoted the volatilization of gasoline droplets, raised the temperature of the unreacted area, and facilitated further reactions with O_2 to generate CO_2. In CO_2 atmosphere, the accumulation of products hindered the oxidation reaction, thereby inhibiting the oxidation of gasoline mist, resulting in a decrease in ΔP_{max} and $(dP/dt)_{max}$. As the volume fraction of inert gas (*n*) continued to increase, the combustion and explosion reactions were influenced by the dilution effect of CO_2 on O_2, as well as the reduction in the rate of elementary reactions [32,33]. In N_2 and Ar atmospheres, the contact areas between free radicals and reactant particles were diminished due to the dilution effects of inert gases on O_2, the flame temperature decreases as a result of the addition of inert gases and so does the reaction rate, which slowed the reaction rate and contributed to the decrease in ΔP_{max} and $(dP/dt)_{max}$.

3.3 Influence of inert gases on flame characteristic parameters

By capturing the flame propagation processes of gasoline cloud in 79 vol. % CO_2 atmosphere, the suppression effects of inert gases on deflagration were further explored, as illustrated in Fig. 6. It was evident that from 0 to 70 ms, the gasoline cloud reacted with O_2. Due to the strong inhibition effect of CO_2, the combustion process of the gasoline cloud was suppressed, and the heat generated in these processes was absorbed by unburned droplets and the wall of the spherical tank. This resulted in the discontinuous propagation of the gasoline flame in CO_2 atmosphere, leading to an irregular flame front shape. The heat produced by the burning droplets preheated other unburnt ones, facilitating the volatilization of additional mist, which resulted in a darker flame propagation process. From 70 ms to 110 ms, as the average temperature in the tank increased, the intensity of the gasoline cloud deflagration also rose, causing the flame to translate into

a continuous phase of propagation. The intense deflagration at t=110 ms made the spherical tank glow brightly. When t>110 ms, the products of the gasoline cloud deflagration contained a significant amount of water and carbon black, which absorbed the heat generated by the reaction. Additionally, the inner wall of the container had a heat absorption capacity, resulting in the observation window gradually becoming dim and blurred.

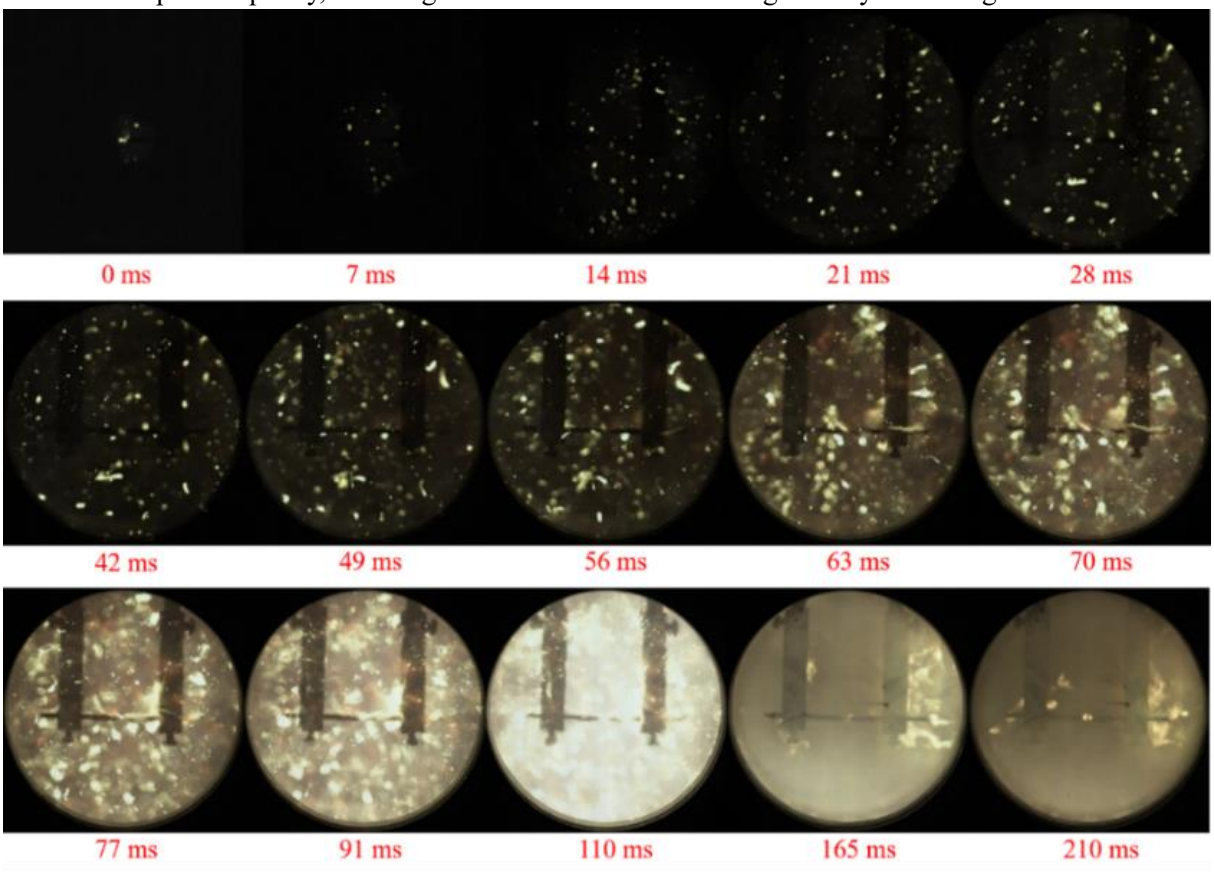

Figure 6. Flame propagation process of gasoline mist explosion under 79 vol. % CO_2 atmosphere.

The colorimetric temperature measurement method based on blackbody radiation theory [34,35] was employed to analyze the flame propagation images captured by a high-speed camera. Fig. 7 illustrated the distribution of the flame temperature field during a gasoline cloud explosion in 79 vol. % CO_2 atmosphere, while Fig. 8 (a) presented the time history curve of the average temperature throughout the combustion processes. From Fig. 7, it was evident that during the initial stage (t=0-70 ms), fragmented high-temperature sparks (primarily droplet micro-explosions) began to emerge, and subsequently, the overall temperature decreased with the average temperature (T_{ave}) dropping from 2020 K to 1588 K. Once the cloud was ignited, the heat generated by the explosion was transmitted through thermal radiation and heat conduction, evolving into a continuous phase flame [33]. This process facilitated the preheating, evaporation, and ignition of unburned droplets around. In the second stage (t=70-110 ms), the volatilized mist explosion caused the flame gradually transition to a continuous phase. The volatilization rate of gasoline increased, allowing more substances to participate in the deflagration reaction, which resulted in a continuous accumulation of heat within the system. Consequently, T_{ave} rose from 1588 K to 2187 K. In the third stage (t>110 ms), the significant accumulation of water and carbon black were produced by the reaction, along with the heat absorption capacity of the container's inner wall, led to the absorption of heat generated by the mist explosion. This resulted in a reduction in the rate of the oxidation reaction, leading to the decline of the average temperature.

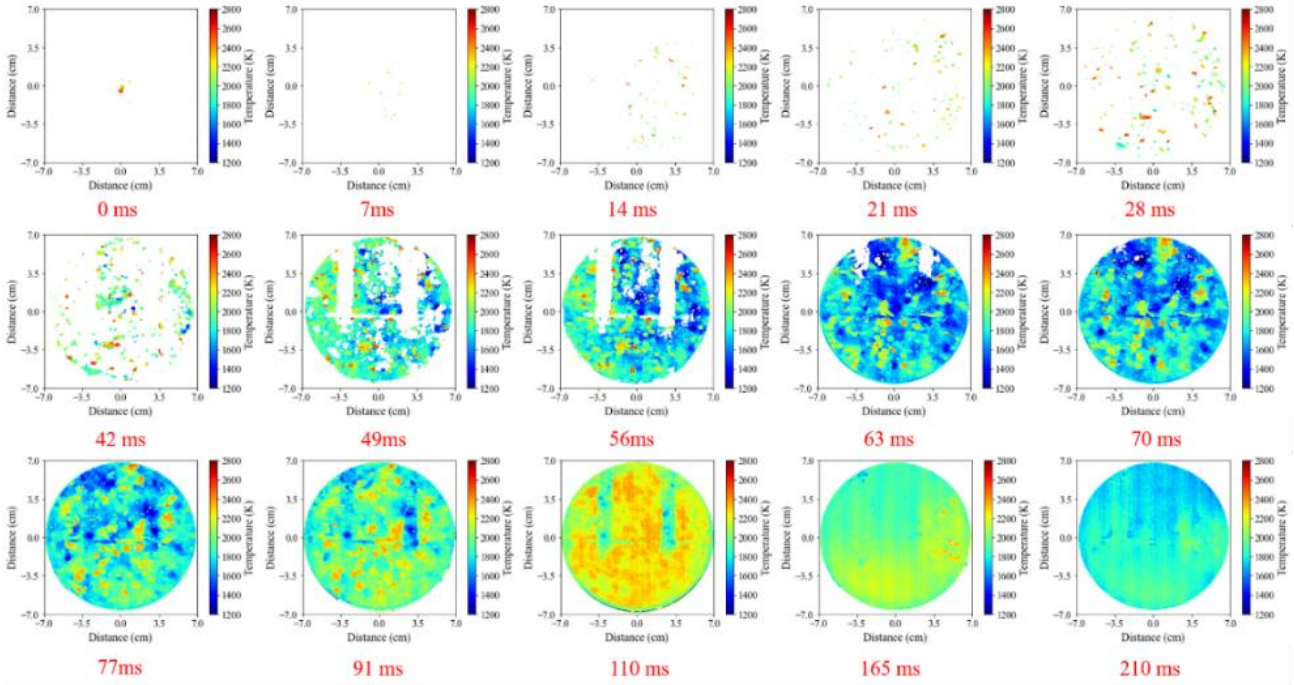

Figure 7. Distribution of flame temperature field of gasoline under CO_2 (n=79 vol. %) atmosphere.

During the initial stage (t=0-17 ms), the micro-explosion of droplets decreased while the mist explosion increased. The flame propagated in a spherical shape, causing the interior of the spherical tank to become progressively brighter. The generated heat preheated the unburned droplets through heat transfer, leading to an increase in the number of preheated droplets and an acceleration in the mist volatilization rate. In the second stage (t=17-26 ms), the preheating of the droplets was nearly complete, resulting in an increase in volatile mist content and a concentrated explosion of the mist. In the third stage (t>26 ms), the products of the mist explosion, such as carbon black and water, absorbed the heat released by the oxidation reaction, which reduced the reaction rate, darkened the flame, and obscured the observation window.

It was evident that the presence of a localized gasoline mist explosions resulted in elevated temperatures, but the average temperature of the spherical tank was primarily influenced by the mist explosion [36].From Fig. 8(b) , it can be seen that in the initial stage (t=0-17 ms), the heat generated by the mist explosion followed the ignition preheated the droplets in the unburned areas and raised the temperature inside the spherical tank, leading to the volatilization of additional mist. This process reduced the average temperature from 1989 K to 1778 K. In the second stage (t=17-26 ms), the preheating of a significant number of droplets was nearly complete, resulting in an increase in mist content within the spherical tank. This accumulation led to a concentrated mist explosion, causing the average temperature to rise rapidly from 1778 K to 2280 K. In the third stage (t>26 ms), the water and carbon black produced by combustion and explosion slowed the rate of the oxidation reaction, resulting in a decrease in the average temperature.

The flame front propagated in a quasi-spherical shape. In the first stage (t=0-10 ms), a significant quantity of ignitable mist was distributed at the flame front, resulting in a substantial increase in the mist explosion area. This enhancement accelerated the rate of oxidation reaction and improved heat transfer efficiency, which in turn increased the rate of mist evaporation from droplets. In the second stage (t=10-18 ms), as the concentration of volatile mist rose, the concentrated mist explosion caused the flame to fill the entire observation window, creating a bright display. In the third stage (t>18 ms), the products of the mist explosion include water and carbon black. Black smoke began to appear in the observation window and gradually obscured the visibility, and the flame itself became increasingly dim.

Figs. 8 (c) show that the increase in local mist explosions raised the flame temperature during the initial

stage (t=0-10 ms). However, the heat generated during this phase was primarily used for preheating the unburned area, resulting in a downward trend in the average temperature, which decreased from 2505 K to 2313 K. The elevated initial temperature accelerated the mist volatilization rate, droplets preheating rate, and overall heat transfer rate throughout the combustion processes, leading to a higher average temperature. It was noteworthy that when the flame front in a high-temperature state propagated to the unburned area, more existing mists would be ignited [37]. These ignited mists generated further heat and accelerated the surrounding oxidation reactions, creating a positive feedback loop that promoted continuous combustion. In the second stage (t=10-18 ms), the agglomerated combustion of droplets and the concentrated explosion of mist caused the average temperature to rise rapidly, increasing from 2313 K to 2586 K. In the third stage (t>18 ms), as the quantity of water and carbon black produced by the reaction gradually increased, the generated heat was absorbed and the rate of the oxidation reaction slowed down, so the average temperature subsequently decreased.

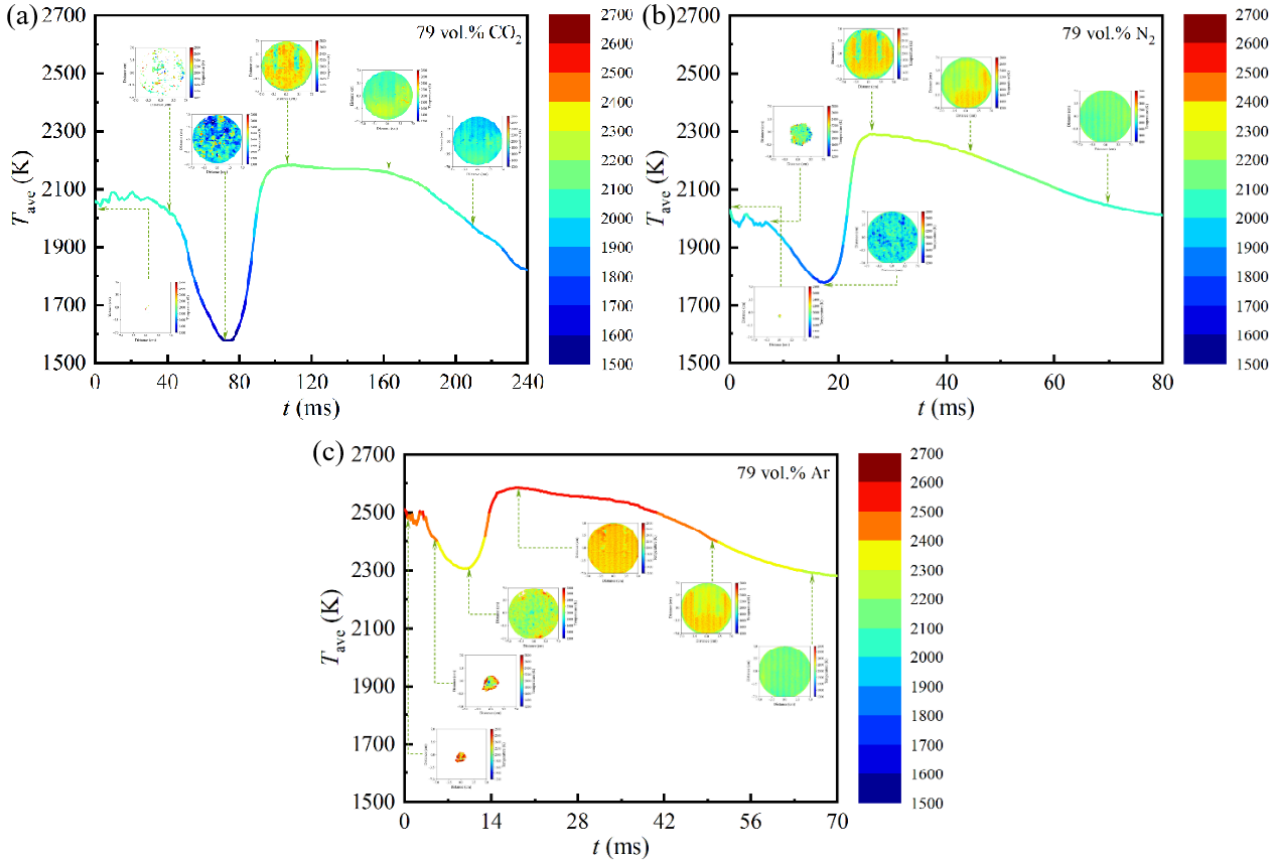

Figure 8. Average flame temperature of gasoline under three atmospheres: T_{ave}&t (a)79 vol. % CO_2; (b)79 vol. % N_2; (c)79 vol. % Ar

As illustrated in Fig. 9, the variation of the maximum average temperature (T_{am}, the maximum T_{ave} value) with the volume fraction of inert gas (n) during the gasoline cloud explosion was presented. The diagram indicated that T_{am} decreased as the volume fraction of inert gas (n) increased across all three inert gas atmospheres. In CO_2 atmosphere, as the volume fraction of inert gas (n) increased from 79 vol. % to 84 vol. %, T_{am} decreased from 2187 K to 1529 K, representing a reduction of 30 %. In N_2 atmosphere, as the volume fraction of inert gas (n) increased from 79 vol. % to 86 vol. %, T_{am} decreased from 2280 K to 1623 K, which corresponded to a decrease of 29 %. In Ar atmosphere, as the volume fraction of inert gas (n) increased from 79 vol. % to 90 vol. %, T_{am} decreased from 2187 K to 1529 K, also reflecting a decrease of 30 %. Within the same range of inert gas volume fractions (n=79 to 84 vol. %), T_{am} decreased from 2184 K to 1525 K in CO_2 atmosphere, resulting in a decrease of 30 %. In N_2 atmosphere, T_{am} decreased from 2280 K to 1947 K, with a

reduction of 14.61 %. In Ar atmosphere, T_{am} decreased from 2586 K to 2395 K, indicating a decrease of 7 %. Compared to the effect on explosion pressure, the addition of inert gas had a more significant impact on the reduction of temperature. The order of the inhibitory effect of inert gas on explosion temperature aligned with that observed for explosion pressure.

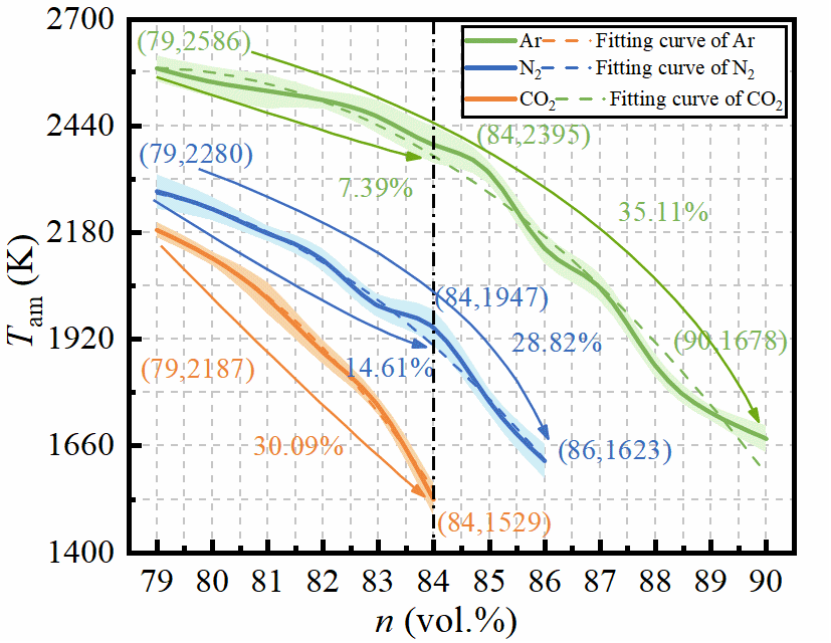

Figure 9. The influence of *n* of three inert gases on T_{am}

The results indicated that CO_2 inhibited flame propagation during the initial stage by absorbing heat due to its high specific heat capacity. This absorption reduced the temperature within the tank, further decreasing the reaction rate and hindering the continuous propagation of local mist. Additionally, CO_2 suppressed the elementary reaction of mist oxidation, impeding the forward progression of the oxidation reaction. This suppression was a key factor contributing to the most significant decrease in average temperature (T_{ave}) during the initial stage. In contrast, N_2 primarily inhibited mist explosions through heat absorption and dilution effect, which mainly affected the preheating process of droplets in the second stage, thereby slowing the heat absorption efficiency and the evaporation rate of unburned droplets. Furthermore, Ar also contributed to the inhibition of mist explosions through heat absorption and dilution, but its effect was relatively weak and resulted in an increased likelihood of mist explosions during the initial stage, leading to a higher average temperature in the tank. Consequently, the evaporation rate of mist and the efficiency of heat transfer to the unburned area were accelerated, resulting in the least decrease in average temperature during the initial stage.

3.4 Discussion of suppression mechanism of inert gases

The explosion process of a gasoline cloud was illustrated in Fig. 10. Initially, gasoline was sprayed into a spherical tank by high-pressure gases, creating a uniform suspended cloud within the tank and volatilizing a significant amount of combustible mist. Subsequently, when an ignition source was introduced, the mist-oxygen mixture was ignited, resulting in a combustion reaction that released light and heat. The heat generated from combustion raised the temperature of the unburned droplets, accelerating the volatilization of the unburned droplet mist and forming a mist-oxygen mixture on the surfaces of droplets. In the reaction zone, droplets, mist, and oxygen coexisted. As the explosion reaction progressed, the continuous diffusion flame transported a substantial amount of heat to the edges of the spherical tank, which in turn pushed the reaction zone and preheating zone toward the boundary of the tank [38].

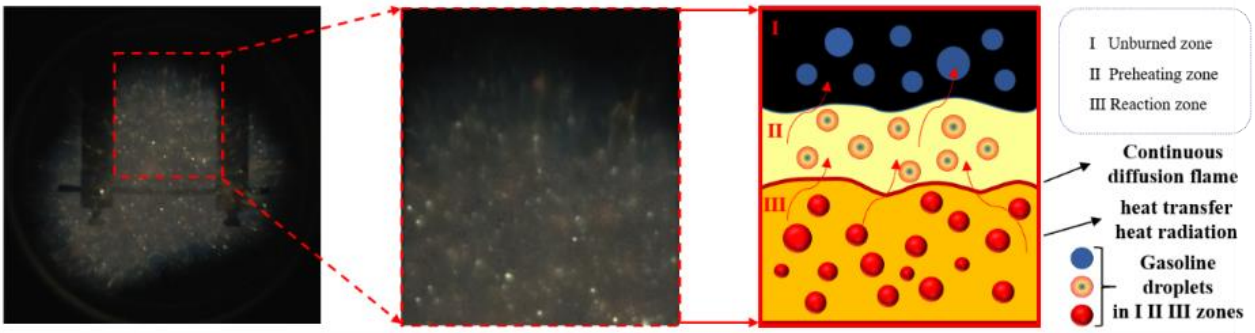

Figure 10. Schematic diagram of gasoline mist explosion model

The introduction of three inert gases (CO_2, N_2, and Ar) effectively inhibited the oxidation reaction, heat transfer, and flame propagation during the combustion and explosion processes, thereby reducing the intensity and hazards associated with the overall combustion and explosion reaction. Fig. 11 illustrated the flame diagram and flame temperature distribution of a gasoline explosion in three different atmospheres at t=14 ms. It was evident that in CO_2 atmosphere, the explosion process remained in the initial stage. CO_2 exerted an inhibitory effect on the elementary reactions involved in gasoline mist oxidation, hindering the effective interaction between the mist-droplet mixture and O_2. As a result, the flame produced by the mist explosion became discontinuous, exhibiting a point-like high-temperature region with uneven distribution within the spherical tank [39,40]. In N_2 atmosphere, the explosion had progressed to the second stage. The flame from the mist explosion filled the observation window, and the heat generated preheated the unburned areas through heat radiation and transfer, but some low-temperature droplets still persist in the region (indicated by blue dots in the image). In Ar atmosphere, the reaction also advanced to the second stage, but the preheating and vaporization processes of the droplets had been completed. Consequently, the number of low-temperature droplets had significantly decreased, while the high-temperature region within the spherical tank had expanded.

CO_2 primarily influenced the initial stage of the explosion reaction by inhibiting the oxidation of gasoline mist, hindering the combination of mist and oxygen, and absorbing a portion of the heat generated during the explosion. These processes resulted in the formation of discontinuous flame areas and diminished the heat transfer effect to the unburned regions [41,42]. CO_2 extended the duration of the mist explosion while simultaneously reduced both the explosion pressure and temperature by impeding mist generation and absorbing explosion heat. In contrast, N_2 and Ar predominantly affected the second stage of the combustion and explosion reaction. In both atmospheres, the initial stage featured a continuous flame, with the flame propagating in spherical and quasi-spherical forms, respectively. By absorbing heat generated from localized mist explosions, the heat transfer rate was diminished, thereby inhibiting the gasoline cloud explosion reaction. Consequently, when the combustion and explosion reaction of the gasoline cloud was entirely suppressed through heat absorption alone, a higher volume fraction of inert gas was required. The heat absorption capacity of N_2 surpassed that of Ar, which enhanced its explosion suppression capability when compared to Ar. In terms of explosion pressure and temperature, the order of inhibitory effects of the three inert gases was as follows: CO_2>N_2>Ar.

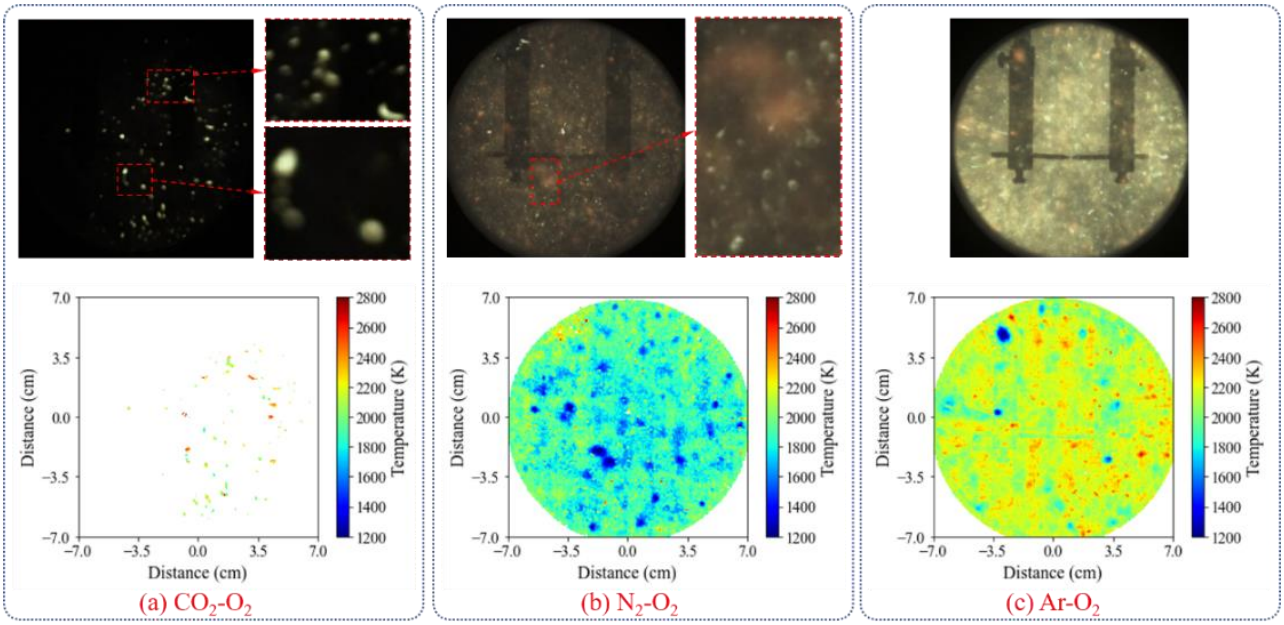

Figure 11. Flame diagrams and flame temperature distribution of gasoline mist explosions in three different atmospheres: (a)CO_2; (b)N_2; (c)Ar

4. Conclusions

In the study, the effects of various types and concentrations of inert gases (CO_2, N_2, Ar) on the explosion characteristics of gasoline cloud were investigated using a 20 L liquid explosion test system. The flame propagation processes, explosion pressure, temperature distribution and reaction mechanisms of gasoline cloud explosions with different inert gases were discussed in detail. The conclusions were as follows:

(1) The n_U of CO_2, N_2, and Ar were 86 vol. %, 88 vol. %, and 92 vol. %, respectively. As the volume fraction of inert gas (n) increased, the maximum pressure (ΔP_{max}), the maximum pressure rise rate $(dP/dt)_{max}$ and the explosion index (K_G) of the gasoline cloud explosion in three atmospheres (CO_2, N_2, Ar) all exhibited a downward trend, while the combustion duration (T_d) showed an upward trend. For the same value of n, the influencing dgrees of ΔP_{max}, $(dP/dt)_{max}$ and K_G for gasoline all followed the order of CO_2<N_2<Ar, whereas T_d exhibited the opposite rule.

(2) Within the respective test concentration ranges, the explosion hazard of the gasoline cloud in the Ar atmosphere transitioned through three stages of St3, St2, and St1. In contrast, the explosion hazards in the CO_2 and N_2 atmospheres were limited to a single stage of St1. The flame propagation processes in the three atmospheres differed significantly. In CO_2 atmosphere, the flame shape was irregular, and the mist explosion generated in the initial stage was suppressed, leading to the segmentation of flame. In N_2 and Ar atmospheres, the flames propagated in spherical and quasi-spherical shapes, respectively.

(3) Furthermore, as the volume fraction of inert gas (n) increased, the maximum average temperature (T_{am}) of the gasoline cloud explosion also exhibited a downward trend. For the same value of n, the T_{am} values followed the order of CO_2< N_2<Ar. CO_2 inhibited free radical reactions and heat absorption, influencing the entire combustion and explosion process. N_2 and Ar primarily affected the second stage of the reaction through their endothermic effects, with N_2 demonstrating a greater endothermic capacity than Ar. Through the analysis of ΔP_{max}, $(dP/dt)_{max}$, K_G, T_d, and T_{am} values of gasoline cloud explosions, the order of explosion suppression effectiveness of the three inert gases on gasoline cloud explosions was CO_2>N_2>Ar.

Acknowledgments

Many thanks to Prof. Ritsu Dobashi, Dr. Po-Jul Chang of the University of Tokyo, for their kindness help with the two-color pyrometer technique. This work was supported by the Natural Science Research Excellent Youth Project of Anhui Educational Committee (No.2023AH020026), the National Natural Science Foundation of China (No.12272001), and the authors would like to thank these foundations for the financial supports.

Declaration of interests

☑The authors declare that they have no known competing financial interests or personal relationships that could have appeared to influence the work reported in this paper.

☐The authors declare the following financial interests/personal relationships which may be considered as potential competing interests:

Reference

[1] Zahlanieh SE, Jean A, Vignes A, et al (2023) A sneak peek into the phenomenology of fuel mist explosions: The key role of vapor fractions. J. Loss Prev. Process Ind 83: 105029. https://doi.org/10.1016/j.jlp.2023.105029

[2] Cai P, Liu ZY, LiM Z, et al (2022) Experimental study of effect of equivalence ratio and initial turbulence on the explosion characteristics of LPG/DME clean blended fuel. Energy 250: 123858. https://doi.org/10.1016/j.energy.2022.123858

[3] Song YF, Zhang Q (2021) Explosion effect of vapor-liquid two-phase n-heptane at various initial temperatures. Process Saf. Environ. Protect 145: 303-311. https://doi.org/10.1016/j.psep.2020.08.021

[4] Mitu M, Brandes E, Hirsch W (2016) Effects of initial temperature and pressure on explosion characteristics of hydrocarbon-air mixtures. J. Loss Prev. Process Ind. 43: 42-52. https://doi.org/10.1016/j.jlp.2016.04.008

[5] Yang P, Wang T, Sheng YH, et al (2024) Recent advances in hydrogen process safety: Deflagration behaviors and explosion mitigation strategies. Process Saf. Environ. Protect 188: 303-316. https://doi.org/10.1016/j.psep.2024.05.111

[6] Song SX, Wang C, Qiao BY, et al (2024) Explosion damage effects of aviation kerosene storage tank under strong ignition. Def. Technol 37: 27-38. https://doi.org/10.1016/j.dt.2023.12.009

[7] Li SZ, Cheng YF, Wang R, et al (2023) Suppression effects and mechanisms of three typical solid suppressants on titanium hydride dust explosions. Process Saf. Environ. Protect 177: 688-698. https://doi.org/10.1016/j.psep.2023.07.039

[8] Yang J, Yu Y, Li YH, et al (2019) Inerting effects of ammonium polyphosphate on explosion characteristics of polypropylene dust. Process Saf. Environ. Protect 130: 221-230. https://doi.org/10.1016/j.psep.2019.08.015

[9] Liu ZQ, Zhong XX, Zhang Q, et al (2020) Experimental study on using water mist containing potassium compounds to suppress methane/air explosions. J. Hazard. Mater 394: 122561. https://doi.org/10.1016/j.jhazmat.2020.122561

[10] Zhang SY, Wen XP, Guo ZD, et al (2023) Effect of N2 and CO2 on explosion behavior of hydrogen-air mixtures in non-premixed state. Fire Saf. J 138: 103790. https://doi.org/10.1016/j.firesaf.2023.103790

[11] Chelliah HK, Wanigarathne PC, Lentati AM, et al (2003) Effect of sodium bicarbonate particle size on the extinction condition of non-premixed counterflow flames. Combust. Flame 134: 261-272. https://doi.org/10.1016/S0010-2180(03)00092-0

[12] Amyotte PR (2006) Solid inertants and their use in dust explosion prevention and mitigation. J. Loss Prev. Process Ind 19: 161-163. https://doi.org/10.1016/j.jlp.2005.05.008

[13] Liang XQ, Zhou XY, Lu X, et al (2024) Investigation on slag resource utilization: KHCO3/modified slag composite powder applied to methane/air explosion suppression. Powder Technol 41: 119814. https://doi.org/10.1016/j.powtec.2024.119814

[14] Mu XM, Cong HY, Shao ZY. et al (2023) Experimental and theoretical research on the inhibition performance of ethanol gasoline/air explosion by C6F12O. J. Loss Prev. Process Ind 83: 105088. https://doi.org/10.1016/j.jlp.2023.105088

[15] Zhang C, Bai CH, Ren JF, et al (2022) The promotion of nitromethane on solid–liquid fuel/air mixtures explosion characteristics under different ambient conditions. Fuel 322: 124190. https://doi.org/10.1016/j.fuel.2022.124190

[16] Abdelkhalik A, Askar E, Markus D, et al (2016) Explosion regions of propane, isopropanol, acetone, and methyl acetate/inert gas/air mixtures. J. Loss Prev. Process Ind 43: 669-675. https://doi.org/10.1016/j.jlp.2016.04.001

[17] Mitu M, Brandes E, Hirsch W (2018) Mitigation effects on the explosion safety characteristic data of ethanol/air mixtures in closed vessel. Process Saf. Environ. Protect 117: 190-199. https://doi.org/10.1016/j.psep.2018.04.024

[18] Mabrouk E, Mourad B (2010) Efficiency of natural and acid-activated clays in the removal of Pb(II) from aqueous solutions. J. Hazard. Mater 178: 1-3. https://doi.org/10.1016/j.jhazmat.2010.02.004.

[19] Wang H, Wu F, Pan XH, et al (2023) Spray and explosion characteristics of methanol and methanol-benzene blends near azeotrope formation: Effects of temperature, concentration, and benzene content. J. Loss Prev. Process Ind 83: 105079. https://doi.org/10.1016/j.jlp.2023.105079

[20] Zhang B, Shen XB, Pang L (2015) Effects of argon/nitrogen dilution on explosion and combustion characteristics of dimethyl ether–air mixtures. Fuel 159: 646-652. https://doi.org/10.1016/j.fuel.2015.07.019

[21] Zhang B, Ng HD (2016) An experimental investigation of the explosion characteristics of dimethyl ether-air mixtures. Energy 107: 1-8. https://doi.org/10.1016/j.energy.2016.03.125

[22] Mukhtar M, Hagos FY, Aziz ARR, et al (2022) Combustion characteristics of tri-fuel (diesel-ethanol-biodiesel) emulsion fuels in CI engine with micro-explosion phenomenon attributes. Fuel 312: 122933. https://doi.org/10.1016/j.fuel.2021.122933

[23] Amyotte P R, Pegg M J, Khan F I. (2009) Explosion characteristics of coal dust-liquid hybrid mixtures: Effects of liquid content and volatility[J]. J. Loss Prev. Process Ind 22: 484-491.

[24] Hu ZL, Zhang YJ, Ai ZY, et al (2024) Hydrogen doping control method for gasoline engine acceleration transient air-fuel ratio. Heliyon 10: e30865. https://doi.org/10.1016/j.heliyon.2024.e30865

[25] Guo Y, Ren K, Huang W, et al (2022) An alternative explosion criterion of combustible dusts based on combustion duration time: applications for minimum explosion concentration and limiting oxygen concentration. Powder Technol 409:117851. https://doi.org/10.1016/j.powtec.2022.117851

[26] Wu D, Krietsch A, Schmidt M, et al (2022) Effect of oxygen concentration, inert gas and CH4/H2 addition on the minimum ignition energy of coal dusts. J. Loss Prev. Process Ind 77: 104772. https://doi.org/10.1016/j.jlp.2022.104772

[27] Li W F, Liu Z C, Wang Z S, et al. 2015. Experimental and theoretical analysis of effects of atomic, diatomic and polyatomic inert gases in air and EGR on mixture properties, combustion, thermal efficiency and NOx emissions of a pilot-ignited NG engine. Energy Conversion and Management. 105: 1082-1095.

[28] Wang C, Song S X, Qiao B Y, et al. 2024. Explosion behaviors of aviation kerosene in a 20 L spherical vessel. Aerospace Science and Technology. 2024: 109308

[29] Lu YW, Fan RJ, Wang ZR, et al (2024) The influence of hydrogen concentration on the characteristic of explosion venting: Explosion pressure, venting flame and flow field microstructure. Energy 293: 130562. https://doi.org/10.1016/j.energy.2024.130562

[30] Cao XY, Zhou JY, Zhou X, et al (2024) Experimental research on the synergy effect of resistance/inhibition on the syngas explosion. Fuel 363: 130995. https://doi.org/10.1016/j.fuel.2024.130995

[31] Qu J, Zhou T, Luo ZM, et al (2024) Research on explosion hazard and prevention of ultrafine aluminium powder based on orthogonal matrix analysis. Process Saf. Environ. Protect 186: 910-920.

https://doi.org/10.1016/j.psep.2024.04.067

[32] Linteris, G. T., et al. (2008). Chemical inhibition of methane-air flames by fire suppressants. Combustion and Flame, 155(1-2), 227–239.和 Westbrook, C. K., Pitz, W. J., & Curran, H. J. (2006). Chemical kinetics of gasoline ignition. Progress in Energy and Combustion Science, 32(3), 283–357.

[33]Chatrathi, K., & Going, J. E. (2001). Flammability limits of combustible gases and vapors in inert atmospheres. Journal of Loss Prevention in the Process Industries, 14(6), 463–474.

[34] Wang ZH, Cheng YF, Mogi T, et al (2022) Flame structures and particle-combustion mechanisms in nano and micron titanium dust explosions. J. Loss Prev. Process Ind 80: 104876. https://doi.org/10.1016/j.jlp.2022.104876

[35] Hu FF, Cheng YF, Zhang BB, et al (2022) Flame propagation and temperature distribution characteristics of magnesium dust clouds in an open space. Powder Technol 404: 117513. https://doi.org/10.1016/j.powtec.2024.120098

[36] Wu F, Wang H, Yu H, et al (2022) Experimental study on the lower explosion limit and mechanism of methanol pre-mixed spray under negative pressure. Fuel 321: 104049. https://doi.org/10.1016/j.fuel.2022.124049

[37] Saneie N, Kulkarni V, Treska B, et al (2021) Microbubble dynamics and heat transfer in boiling droplets. Int. J. Heat Mass Transfer 176: 121413. https://doi.org/10.1016/j.ijheatmasstransfer.2021.121413

[38] El-Zahlanieh S, Santos ISD, Sivabalan S, et al (2022) Finding a way through the “misty” evaluation of the flammability and explosivity of kerosene aerosols. Fuel 328: 125275. https://doi.org/10.1016/j.fuel.2022.125275

[39] Zhang SY, Wen XP, Guo ZD, et al (2023) Experimental study on the multi-level suppression of N2 and CO2 on hydrogen-air explosion. Process Saf. Environ. Protect 169: 970-981. https://doi.org/10.1016/j.psep.2022.11.069

[40] Liu QQ, Liu LQ, Liu ZY, et al (2024) Effects of H2 blended ratio and N2/CO2 dilution fraction on the deflagration shock wave of H2NG in slender closed pipelines. Int. J. Hydrogen Energy 73: 451-461. https://doi.org/10.1016/j.ijhydene.2024.06.072

[41] Wu WY, Wei AZ, Huang WX, et al (2021) Experimental and theoretical study on the inhibition effect of CO2/N2 blends on the ignition behavior of carbonaceous dust clouds. Process Saf. Environ. Protect 153: 1-10. https://doi.org/10.1016/j.psep.2021.07.005

[42] Wu DJ, Tan X, Wei AZ, et al (2021) Ignition temperature and mechanism of carbonaceous dust clouds: The roles of volatile matter, CH4 addition, O2 mole fraction and diluent gas. J. Hazard. Mater 405: 124189. https://doi.org/10.1016/j.jhazmat.2020.124189

Paper submitted: 14.05.2025

Paper revised: 07.07.2025

Paper accepted: 11.07.2025